醫工學會誌 : 第10卷, 第 3 號, 1989
J. of KOSOMBE : Vol. 10, No. 3

研 究 論 文
89− 3 −11

Image Restoration in Digital Radiography Using Dual Sensor Wiener Filer

Tae Soo Lee, Kwang Suk Park, Byoumg Goo Min, Jeong Gee Lim, Man Chung Han

−Abstract−

A Dual Sensor Wiener Filter technique was used to improve the image quality of the scanning type digital radiographic system (resolution and SNR). In this method, two images were acquried simultaneously using two sensors with high and low resolution and SNR values. Using the cross power spectrum between dual sensor outputs of the same chest radiographic image, we design a new type of Wiener Filter and implement it with fast algorithm. We compared the performance of this new dual sensor filter with conventional single sensor filters (Wiener Filter and Parametric Projection Filter). In simulation studies, it is shown that this new method has SNR improvement of 1−3 dB better than conventional filters.

1. Introduction

In digital radiography (DR), a X−ray image is displayed on computer graphic screen in digital format, and it has many merits of better image contrast and more diagnostic informations through image processing than conventional screen film system.[1] In the image processing of digital radiography, there are two typical methods, such as image contrast enhancement and image restoration. Since the image contrate enhancement of DR image emphasizes minute difference of contrast or fine details using histogram equalization[2] or unsharp masking[3][4], it can provide psychovisually enhanced image for human observer, but it may allow significant reduction of other diagnostic informations. Image restoration process reduces the degraded effects in the acquired images which can be degraded by electrical and quantum noise and blurred by modulation transfer function of system [5].

Two parameters indicating the performance of digital radiograpic system are resolution and signal to noise ratio (SNR)[6], which have competitve relation each other, therefore optimal trade−off is required for improving one without degrading the other significantly. Wiener filter is a typical restoration filter which is optimal in the sense of Minimum Mean Square Error criterion[7]. In this paper, we extend the conventional single sensor Wiener Filter concept to dual sensors case and propose a new type filter which processes two images simultaneously with a fast algorithm. Dual Sensor Wiener Filter is based on multi−channel image processing with an extension of multi−channel signal processing method to 2−dimension[8]. Since we

〈접수 : 1989년 11월 13일〉
The part of this paper was presented at 1lst Scientific Assembly and Annual Meeting of RSNA, Nov.1985
Institute of Biomedical Engineering
Cepartment of Biomedical Engineering and Radiology
College of Medicine, Seoul National University

used only two channel signals, the multi－channel problem is simplified and it becomes possible to investigate the effect of inter －channel spectrum on the filter parameters. We evaluated this new filter method using the DR images with various levels of blurring and noise. We compared its performance with that of conventional single sensor Wiener filter and parametric projection filter (PPF')[9]

2. Model of Imagng System

In a discrete and linear shift invariant (LSI) system, unknown original imge, f(i,j), is degraded to the measured image, g(i, j) by point spread function, h(i, j), and additive noise, n(i, j). Then g(i, j) can be represented by Eq. (1).

$$g(i, j)=\sum_{m=0}^{M-1}\sum_{m=0}^{M-1} f(m, n)\ h(i-m, j-n)+n(i, j) \qquad (1)$$

where the image size is M x M.

This equation becomes Eq. (2) in vector－matrix form with column stacking as Eq. (2).

$$g=H\ f+n \qquad (2)$$

where g, f and n are M^2 x 1 vectors and H is M^2 x M^2 matrix with Block Toeplitz form. In the case of dual sensor, each sensor has M x M image size and the above vectors and matrix can be represented by Eq. (3)

$$g=\begin{bmatrix} g_1 \\ g_2 \end{bmatrix} \quad f=\begin{bmatrix} f_1 \\ f_2 \end{bmatrix} \quad H=\begin{bmatrix} H_1 & \underline{O} \\ \underline{O} & H_2 \end{bmatrix} \quad n=\begin{bmatrix} n_1 \\ n_2 \end{bmatrix} \qquad (3)$$

Our purpose is to estimate optimal f from g assuming that MTF of system and some properties of g and n, such as mean and variance, are known a priori. Image model and filter can be summarized as Fig. 1

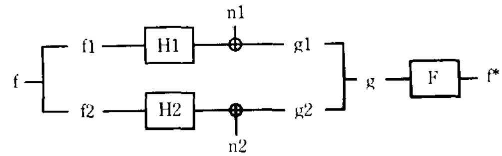

Fig. 1 Bock diagram of Image model and Filter

3. Dual Sensor Wiener Filter

In a linear system, let the measured image be g and image filtered by linear filter A be $\overset{*}{f}$, then Wiener filter minimizes mean square error $E\{|f-\overset{*}{f}|^2\}$ and the filtered image is represented by Eq. (4).

$$f^* = R_f H^t [H\ R_f H^t + R_n]^{-1} g \qquad (4)$$

where R_f and R_n are autocorrelation matrices of the original image and noise, respectively.

$$R_f=\begin{bmatrix} R_{f11} & R_{f12} \\ R_{f21} & R_{f22} \end{bmatrix} \quad Rn=\begin{bmatrix} R_{n11} & \underline{0} \\ \underline{0} & R_{Rn22} \end{bmatrix} \qquad (5)$$

In the estimation of the optimal solution of Eq. (4), the most important calculation is matrix inverse of $R=HR_fH^t+R_n$, whose size is $2M^2 \times 2M^2$. where,

$$R=HR_fH^t+R_n$$

$$=\begin{bmatrix} H_1R_{f11}H_1^t+R_{n11} & H_1R_{f12}H_2^t \\ H_2R_{f21}H_1^t & H_2\ R_{f22}\ H_2^t+R_{n22} \end{bmatrix} \qquad (6)$$

But it is nearly impossible to calculate directly.

In the case that cross correlation matrix of two images f_1 and f_2 are zero, that is when two images are independent one another, the off diagonal submatrices of R_f are zero matrices. Therefore the Wiener filtered images $\dot{f}_1$ and f_2 are represented by Eq. (7).

$$R_f=\begin{bmatrix} R_{f11} & \underline{O} \\ \underline{O} & R_{f22} \end{bmatrix}$$

which are the same as the result of conventional single sensor wiener filter.

$$f_1 = R_{f11}H_1^t[H_1 R_{f11}H_1^t + R_{n11}]^{-1}g_1$$
$$f_2 = R_{f22}H_2^t[H_2 R_{f22}H_2^t + R_{n22}]^{-1}g_2 \qquad (7)$$

In this paper, because we assumed that the two images are acquired in the same area by two sensors with different resolution and SNR, the off-diagonal submatrices of R_f cannot be zero but have large correlation values. So the calculation of inverting R in Eq. (6) is very complicated.

4. Algorithm

To calculate inverse of R simply using fast algorithm such as FFT, we map vectors to frequency domain. (10)

$$F = \bar{W}^{-1}f \quad f = \bar{W}F \qquad (8)$$

where $\bar{W}$ is two dimensional block DFT matrix with size of $2M^2 \times 2M^2$, and W is 2D-DFT matrix with size of $M^2 \times M^2$

$$\bar{W} = \begin{bmatrix} W & \underline{O} \\ \underline{O} & W \end{bmatrix} \quad \bar{W}^{-1} = \begin{bmatrix} W^{-1} & \underline{O} \\ \underline{O} & W^{-1} \end{bmatrix}$$

$$W = [W_{ij}] \; i, j = 0, 1, \cdots\cdots, M-1$$

$$W_{ij} = w_{ij}[w_{kl}] \; k, l = 0, 1, \cdots\cdots, M-1$$

$$w_{mn} = \exp\left(j\frac{2\pi mn}{M}\right)$$

In the same way, the point spread function matrix H and correlation matrices R_f, R_n are mapped and Eq.(4) can ve represented by Eq. (9).

$$\bar{W}^{-1}\overset{*}{f} = \bar{W}^{-1}R_fH^t[H R_fH^t + R_n]^{-1}g$$
$$= \bar{W}^{-1}R_f\bar{W}\bar{W}^{-1}H^t\bar{W}\bar{W}^{-1}[H R_fH^t + R_n]^{-1}g$$
$$= [\bar{W}^{-1}R_f\bar{W}]\bar{W}^{-1}H^t\bar{W}][\bar{W}^{-1}(H R_f H^t + R_n)^{-1}\bar{W}]G \qquad (9)$$

where matrix H with Block Toeplitz form can be approximated by Block Circulant matrix form, assuming that the edge effect of filtered image may be ignored. Then it can be decomposed into diagonalized eigen value matrix and eigen vector matrix which has the form of Fourier transform matrix and be represented by Eq. (10). Therefore we can use fast algorithm such as Fast Fourier Transform (FFT).

$$\bar{W}^{-1}H^t\bar{W} = \begin{bmatrix} W^{-1}H_1^tW & \underline{O} \\ \underline{O} & W^{-1}H_2^tW \end{bmatrix} \qquad (10)$$

Here R_f is not Block Toeplitz, and it is impossible to diagonalize. However, in stationary process, the submatrices of R_f (R_{f11}, R_{f12}, R_{f21}, R_{f22}) are all Block Toeplitz. Using this property, we can decompose Eq. (9), where R_f can be represented as block matrix of diagonalizable submatrices like Eq. (11) and R of Eq. (6) can be mapped as Eq. (12).

$$\bar{W}^{-1}R_f\bar{W} = \begin{bmatrix} W^{-1}R_{f11}W & W^{-1}R_{f12}W \\ W^{-1}R_{f21}W & W^{-1}R_{f22}W \end{bmatrix} \qquad (11)$$

$$\bar{W}^{-1}R\bar{W} = \begin{bmatrix} W^{-1}[H_1 R_{f11}H_1^t + R_{n11}]W & W^{-1}[H_1R_{f12}H_2^t]W \\ W^{-1}[H_2 R_{f21}H_1^t]W & W^{-1}[H_2 R_{f22}H_2^t + R_{n22}]W \end{bmatrix} \qquad (12)$$

Here the eigen value matrix of R_{ij} has diagomal term with 2 dimensional DFT coefficient of R_{ij}, corresponding to submatrix of 2D power spectrum of f, and representig it as S_{ij} yields Eq(13).

$$W^{-1}R_{n11}W = S_{n11} \qquad W^{-1}R_{n22}W = S_{n22}$$
$$W^{-1}R_{f11}W = S_{f11} \qquad W^{-1}R_{f22}W = S_{f22}$$
$$W^{-1}R_{f12}W = S_{f12} \qquad W^{-1}R_{f21}W = S_{f21} \qquad (13)$$

Therefore Eq. (9) can be written as Eq. (14).

$$\overset{*}{F} = \begin{bmatrix} S_{f11} S_{f12} \\ S_{f21} S_{f22} \end{bmatrix} \begin{bmatrix} H_1^* & \underline{O} \\ \underline{O} & H_2^* \end{bmatrix} \begin{bmatrix} H_1 S_{f11} H_1^* + S_{n11} & H_1 S_{f12} H_2^* \\ H_2 S_{f21} H_1^* & H_2 S_{f22} H_2^* + S_{n22} \end{bmatrix}^{-1} \begin{bmatrix} G_1 \\ G_2 \end{bmatrix} \qquad (14)$$

In calculating Eq. (13), the submatrices of Eq. (13) are all diagonalized form and Eq. (14) can be simplified as Eq. (15), where $F_1(m, n)$ and $F_2(m, n)$ are scalar 2D spectrum of $f_1(i, j)$ and $f_2(i,j)$, respectively. In this form, the order of operation unmber is not $M^2 \times M^2$ but M^2

$$\overset{*}{F}(m, n) = \begin{bmatrix} F_1^*(m, n) \\ F_2^*(m, n) \end{bmatrix} \tag{15}$$

$$= \frac{1}{1 + |H_1(m, n)|^2 \dfrac{S_{f11}(m, n)}{S_{n11}(m, n)} + |H_2(m, n)|^2 \dfrac{S_{f22}(m,n)}{S_{n22}(m, n)}} \times$$

$$\begin{bmatrix} H_1^*(m, n) \dfrac{S_{f11}(m, n)}{S_{n11}(m, n)} G_1(m, n) + H_2^*(m, n) \dfrac{S_{n22}(m, n)}{S_{f22}(m, n)} G_2(m, n) \\ H_1^*(m,n) \dfrac{S_{f21}(m, n)}{S_{n11}(m, n)} G_1(m, n) + H_2^*(m, n) \dfrac{S_{f22}(m, n)}{S_{n22}(m, n)} G_2(m, n) \end{bmatrix}$$

As compared with the dual sensor filter of Eq. (15), conventional Wiener filter can be represented as Eq. (16).

$$\overset{*}{F}(m, n) = \frac{\overset{*}{H}(m,n) \dfrac{S_f(m, n)}{S_m(m, n)} G(m, n)}{1 + |H(m, n)|^2 \dfrac{S_f(m, n)}{S_n(m, n)}} \tag{16}$$

$$= \frac{H\ (m, n)\quad S_f(m, n)\quad G(m, n)}{|H(m, n)|^2\ S_f(m, n) + S_n(m, n)}$$

Comparing Eq. (15) with Eq. (16), we can see the difference between conventional Wiener Filter and dual Sensor Wiener Filter (DSWF). In DSWF, the numerator is a weighed sum of $G_1(m, n)$ and $G_2(m, n)$, where the weighted factor has the components of auto power specrum or cross power spectrum. The denominator has also two components corresponding to each sensor.

5. Simulation

To test performance of new type Dual Sensor Wiener Filter, we acquired a chest X－ray image using a linear photodiode array digital radiography which was developed for research in our laboratory. The image result of this system is 1024x1024 pixels with 256 grey levels. Using this image as original image, the simulation images were obtained by degrading it with various point spread functions and noise levels. After we filtered them with DSWF, SSWF and PPF, we compared the output SNR's of the corresponding images. Fig.2 is the original chest X－ray image. This image is subsampled by two for 256 x 256 resolution to be used in the simulation study. The blurring effect of the

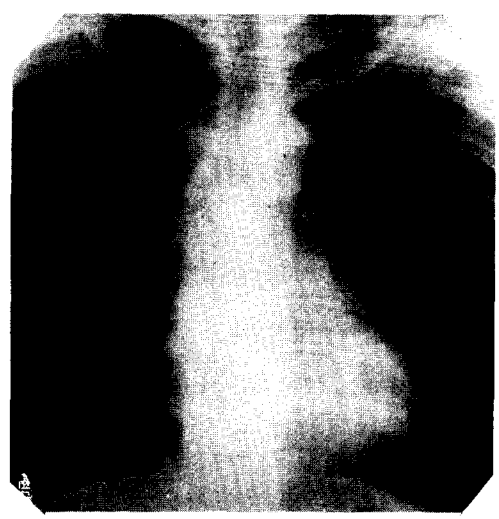

Fig. 2 Original chest X－ray image for simulation (512 x 512 resolution with 256 gray levels)

system was simulated by using circular convolution with the original image and the point spread function of Gaussian form in frequency domain. Then the level of the blur effect is represented by standard deviation of two dimensional Gaussian curve. Fig.3 shows the various modulation transfer function (MTF) of the simulated system with various blurring properties. As we can see in Fig.3, MTF's for this simulation have nearly zero values at the Nyquist frequency ranges and the point spread matrix H is singular. To simulate noise effect, we generate pseudo white gaussian noise with various level and add them to blurred images. In this simulation study, we made simulation images with various MTF's and SNR's as table 1. Simulation images are shown in Fig. 4

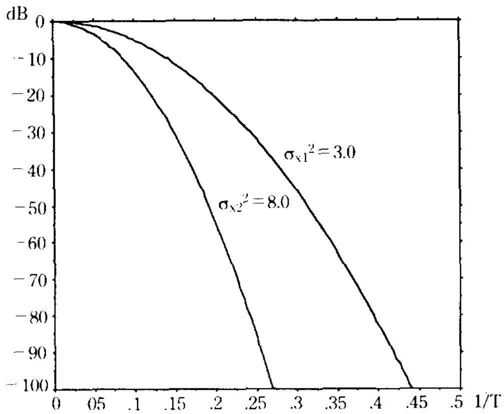

Fig. 3 modulation Transfer Functions with Gaussian Pont Spread Function

Table 1. Blurring parameters of Degraaed images for simulation study

Image	σ_x^2, σ_y^2	σ_n	SNRi (dB)
Image 1	3.0	8.0	15.01
Image 2	3.0	20.0	7.94
Image 3	8.0	8.0	14.32
Image 4	8.0	20.0	7.79

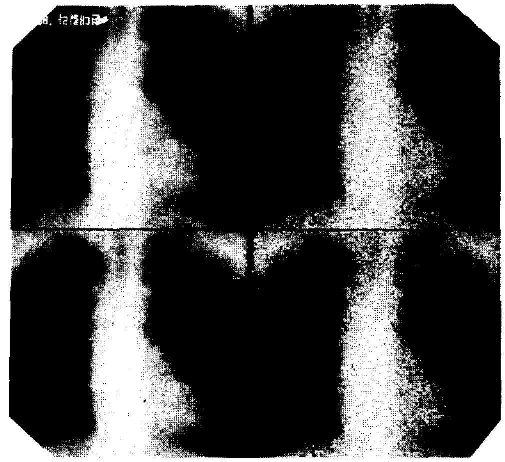

Fig. 4 Blurred images with Table 1 blurring parameters
image 1 : upper left image 2 : upper right
image 3 : lower left image 4 : lower right

In the design of filter, the power spectrum of additive noise is assumed to be white Gaussian noise, so its power level can be calculated from input variances of images. But, in practice, the noise generated in computer is not ideal white Gaussian and Eq, (17) is used to estimate noise power level, where weighted factor (wf) is about o.61 when M is 256.

$$S_{n1}=\sigma_{n1}^2 \times M \times M \times wf$$
$$S_{n2}=\sigma_{n2}^2 \times M \times M \times wf \quad (17)$$

In all simulation studies, we calculate noise level using Eq. (17). The power spectrum of unknown original image is estimated from the power spectrum of the degraded images, using windowed periodogram method (11),
where the Hamming window was used and represented by Eq. (18) as shown in Fig.5.

$$HW(i) = 0.538 + 0.462\cos\left(2\pi\left(\frac{i}{M-1} - 0.5\right)\right) \quad (18)$$

$HW(i,j) = HW(i) \times HW(j)$ for $i,j=0, 1, \cdots\cdots, M-1$

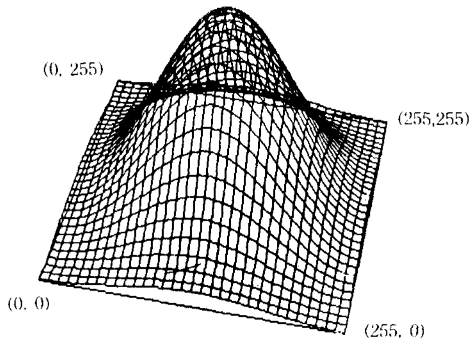

Fig. 5 2－D Hamming Window used for estimation of Power Spectrum

To compare the performance of new filter, we use conventional WF and PPF. Parametic Projection Filter minimizes J(A), which is composed of mean square error and weighted noise component of the restored image, (10)

$$J(A) = tr\{(I-AH)(I-A'H')\} + \gamma\, tr\{A R_n A'\} \quad (19)$$

and is expressed as Eq (20) and is known to have better performance than WF when the blurring effect is dominant in images. Comparing Eq. (20) with Eq. (16), we can see that γ corresponds to inverse term of $s_i(m, n)$. We can adjust ill condition adjusting parameter γS_n, such that PPF have optimal performance. Input parameters of PPF in 4 images are summarized in Table 2.

$$\overset{*}{F}(m, n) = \frac{\overset{*}{H}(m, n)\, G(m, n)}{|H(m, n)|^2 + \gamma\, Sn(m, n)} \quad (20)$$

Table 2. Parameter of PPF for 4 images (NSR noise to signal ratio constant)

Image 1	γ	NSR	$\|I-AH\|^2$	$\gamma\|AR_nA'\|^2$
Image 1	0.500×10^{-7}	0.05	0.450	0.013
Image 2	0.625×10^{-8}	0.10	0.460	0.012
Image 3	0.500×10^{-7}	0.05	0.483	0.005
Image 4	0.625×10^{-8}	0.10	0.487	0.005

6. Result

In the application of Dual Sensor Wiener Filter, three types of image pair were used. According to the image pair to be processed simultaneously, Dual sensor filter is named as DSWF1, DSWF2, and DSWF3. DSWF1 uses image pairs with the same level of blurring and DSWF2 uses image pair with the same level of additive noise and DSWF3 use image pairs with different levels of blurring and noise. The relation between three types of Dual Sensor Filter and four degraded images is shown in Fig.6.

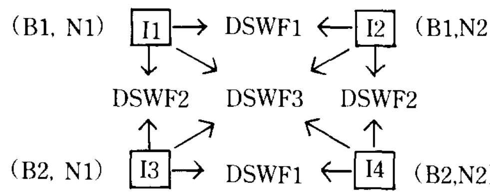

I1,I2,I3,I4 : Image 1, 2, 3, 4
B1, B2 : Blurring Levels
N1, N2 : Noise Levels

Fig.6 Relation between Filter and Image

To compare the performance of filters, the improvement factor was estimated by calculating the difference of input and output SNR represented by Eq. (21).

$$SNR(dB) = 10Log \frac{\sum_{j=0}^{N-1}\sum_{i=0}^{N-1} f(i, j)^2}{\sum_{j=0}^{N-1}\sum_{i=0}^{N-1} \{f(i, j) - g(i, j)\}^2} \quad (21)$$

In Eq. (21), we let N be 240, which is smaller than image size, to remove edge effect in calculating improvement factor, since the block circulant approximation of the block toeplitx matrix has error in the edge region. The calculated improvement factors of four different images and five ty-

Table 3. Improvement factor ¼dB¾ in SNR⅜s of filtered output images

	DSWF1	DSWF2	DSWF3	WF	PPF
F1	4.79	5.04	4.81	3.97	2.20
F2	10.14	9.73	9.93	8.74	4.95
F3	4.23	5.08	4.29	3.45	4.11
F4	10.03	9.54	9.98	8.07	7.13

pes of filters are summarized in Table 3.

As we see in Table 3, the performance of DSWF is different depending upon the image pair used but it is shown to be better than those of WF and PPF. Interesting result is that the difference between the improvement factor of DSWF and WF is dependent upon the SNR difference of image pair used. The relation of two SNR differences are shown in Fig. 7. Besides, the performance of single sensor wiener filter is better than that of PPF when image has less blur and more noise. On the other thank, PPF output is better than WF when

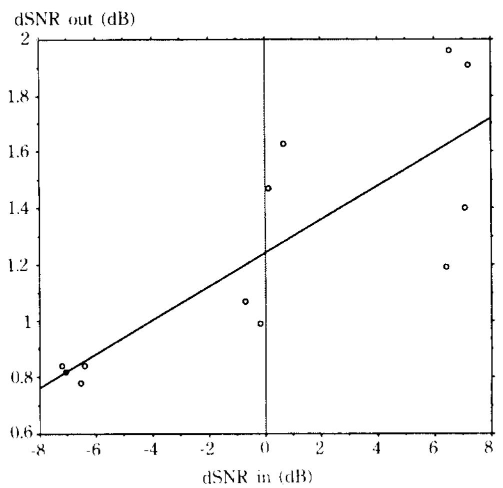

Regression Output

constant	1.241666	Degrees of Freedom	10
Std Err of Y Est	0.259210	X Coefficient(s)	0.059752
R Squared	0.259210	Std Err of Coef.	0.012440
No. of Ovservations	12		

Fig. 7 Relation of dSNR in and dSNR out

image has more blur and less noise. Fig. 8 is filtered output of image 1. In WF image, the blurring effect is dominant and, in PPF image, the noise artifact is shown to be significant. But, in DSWF1 and DSWF2 images, the blurring and noise artifact are not visible. Fig. 9—11 are filtered output of images 2—4 respectively. Fig. 12 is DSWF3 output of Fig. 4

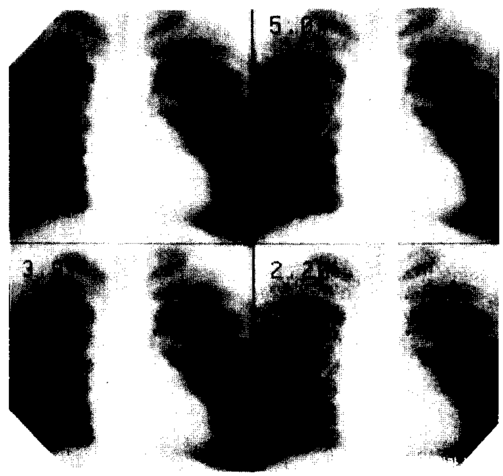

Fig. 8 Filter output of image 1
DSWF1 : upper left DSWF2 : upper right
WF : lower left PPF : lower right

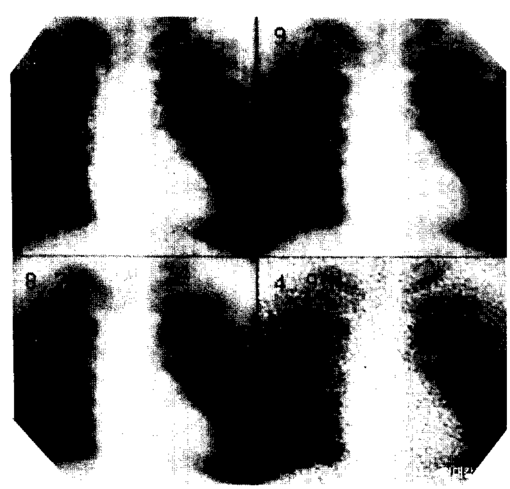

Fig. 9 Filter output of image 2

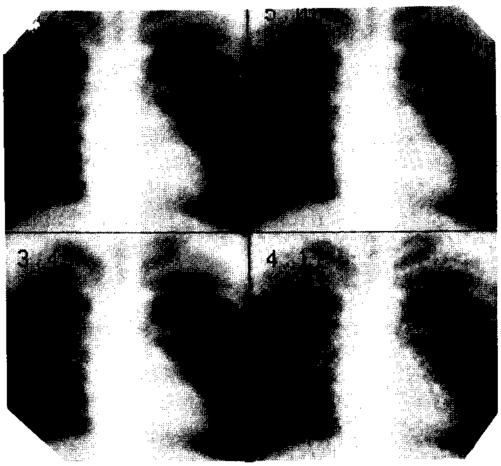

Fig.10 Filter output of image 3

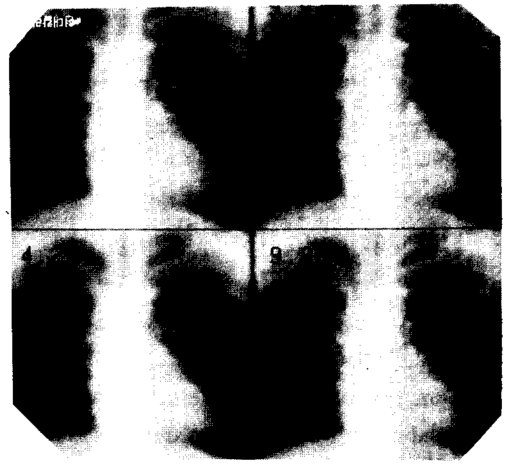

Fig.12 DSWF3 output of Fig.4

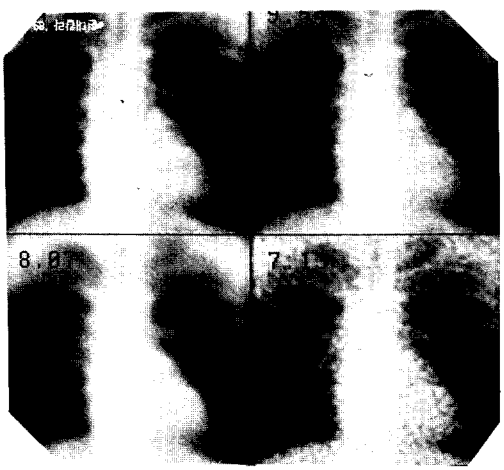

Fig.11 Filter output of image 4

7. Conclusion

The effectiveness of image processing algorithm in digital radiography was shown statistically using subjective characteristics of radiologists [12], such as ROC (receiver operating characteristics) curves. [13][14]. Since the objective of this paper is the restoration of degraded image, we use the objective parameter indicating the effectiveness of processing algorithm. In this method, it can be shown by the mean square error (MSE) between the estimated image and the original image in simulation.

In this case, the level of edge preservation is affected by the estimated magnitude of additive noise. As we can see in the simulation study, the proposed new type filter has less MSE than conventional WF and PPF by about 2 times, depending upon the noise and blurring characteristics of the simultaneously processing image pair to be used.

For the improvement factor of DSFWcompared with WF, it is shown that the larger the difference of SNR of the image pair, the larger the difference of improvent factor between DSWF and WF. Therefore, we can conclude that we can apply this filter effectively to the system with two sensors with different characteristics. In digital radiography, we can acquire different images, according to the level of X－ray energy or characteristics of sensors. Specially, Dual energy imaging technique in DR is very useful to study tissue and bone separated images (15), but introduces noise artifact and needs image restoration method.

In this paper, we only consider two images of the same area and size. But the two images in the same size with different area or two images in the same area with different size may be used as imag pair. In this case, a sophisticated spectrum estimation algorithm has to be used for reliable restoration. We do not consider different local characteristics of image but calculate power spectrum of total image. Since the chest image has different characteristics in each local region, such as lung field and mediastinum, and adaptive application of DSWF in each local region will produce a better performance.

Reference

1) J.S.Daponte and M.D. Fox, "Enhancement of Chest Radiographs with Gradient Operators", IEEE Trans. Med. Imaging 7, 109−117 (19 88)
2) J.B. Zimmerman, S.M. Pizer, E.V.Staab, J.R. Perry, W.Mccartney, B.C.Brenton, "An Evaluation of the Effectiveness of Adaptive Histogram Equalization for Contrast Enhancement", IEEE Trans. Med Imaging 7, 304−312 (1988)
3) M.I Sezan and A.M.Tekalp. "Automatic Anatomically Selective Image Enhancement in Digital Chest Radiography", IEEE Trans. Med. Imaging 8, 154−162 (1989)
4) M.I.Giger and Kunio Doi, "Investigation of Basic Imaging properties in Digital Radiography. 4. Effect of Unsharp Masking on the Detectabilty of Simple Patterns", Med. Phys. 12, 209−214 (1985)
5) M.L.Giger and Kunio Do. "Investigation of Basic Imaging Properties in Digital Radiography. 1. Modulation Transfer Function", Med. Phys. 11, 287−295 (1984)
6) M.L.Giger and Kunio Doi, "Investigation of Basic Imaging Properties in Digital Radiography. 3. Effect of Pixel Size on SNR and Threshold Contrast", Med. Phys. 12, 201−208 (1985)
7) H.C.Andrews and B.R.Hunt, Digital Image Restoration, (Prentice Hall, 1977)
8) N.P.Galatsanos and R.T.Chin, "Digital Restoration of Multi−Channel Images", IEEE Trans. ASSP−37, 415−421 (1989)
9) Erkki Oja and Hidemitsu Ogawa, "Parametric Projection Filter for Image and Signal Restoration", IEEE Trans. ASSP−34, 1643−1653 (1986)
10) R.C.Gongalez and Paul Wintz, Digital Image Processing, (Addison−Wesley Publishing, 19 77)
11) S.L.Marple Jr., Digital Spectrum Analysis with Applications, (Prentice−Hallm 1987)
12) G.L.Anderson and A.N.Netravali, "Image Restoration Based on a Subjective Criterion", IEEE Trans. SMC−6, 845−853 (1976)
13) C.E.Metz, "ROC Methodolgy in Radiologic Imaging", Invest, Radiol.21, 720−733 (1986)
14) H.P.Chan, C.J.Vyborny, H.MacMahon, C.E. Metz, Kunio Doi, E.A.Sickles, "ROC Studies of the Effect of pixel Size and Unsharp Mask Filtering on the Detection of Subtle microcalcifications", Invest, Radio. 22,581−589 (1987)
15) D.F.Morgan, R.A.Sones, and G.T.Barnesm "Performance Characteristics of a Dual Energy Detector for Digital Scan Projection Radiography", Med. Phys. 14, 728−735 (1987)